Deflecting flexural wave with high transmission by using pillared elastic metasurface

Liyun Cao, Zhichun Yang, Yanlong Xu, Badreddine Assouar

Deflecting flexural wave with high transmission by using pillared elastic metasurface

Liyun Cao[1], Zhichun Yang[1], Yanlong Xu[1], Badreddine Assouar[2]

[1]School of Aeronautics, Northwestern Polytechnical University, Xi'an, 710072, China

[2]CNRS, Institut Jean Lamour, Vandoeuvre-lès-Nancy F-54506, France and Université de Lorraine, Institut Jean Lamour, Boulevard des Aiguillettes, BP: 70239, Vandoeuvre-lès-Nancy 54506, France

E-mail: yangzc@nwpu.edu.cn and xuyanlong@nwpu.edu.cn

Abstract

This paper proposes an innovative and simple elastic metasurface, which is one kind of ultrathin metamaterials, to abnormally deflect vertical and oblique incident flexural waves. In particular, negative refraction of flexural wave is also realized. The proposed metasurface can support the capabilities of high transmission and full phase control for transmitted waves. The metasurface is composed of three-dimensional (3D) functional units which are combined with multiple slender pillars for phase shift accumulation. The slots are filled in the 3D functional units to avoid coupling between adjacent functional units. Firstly, based on the generalized Snell's law, the metasurface in the sub-wavelength regime is theoretically designed. Secondly, the deflecting functionality of the metasurface for incident flexural waves is numerically demonstrated. Finally, the deflecting functionality is verified by the corresponding experiments. The proposed metasurface has a great application potential in many fields, such as ultrasonic detection, energy harvesting, and vibration control.

Keywords: metasurface, metamaterials, flexural wave, wave propagation, refraction, ultrasonic detection

1. Introduction

Metasurface, one kind of ultrathin metamaterials within a more compact and easily fabricated form, was recently proposed to realize the extreme features of bulky metamaterials [1-4]. The studies on the metasurface with phase discontinuities, based on the generalized Snell's law (GSL) [5], have made a significant progress in the fields of optics [5-7] and acoustics [8-11]. However, subsequent development field of elastic metasurface is relatively weak. The main reason is that the vector nature of elastic waves makes the elastic metasurface more complex to design than the optic and acoustic ones, in spite of providing richer underlying physics.

Among the existing studies of the elastic metasurface [12-19], the approaches of adjusting wave phase shift can be reduced to three types: changing the wave velocity [12-14], changing the propagation distance [15, 16], and tuning local resonance [17-19]. In the current study, we only consider the elastic plate wave metasurface. For designing a metasurface, the aforementioned first type usually needs multiple kinds of materials, and the second one will enormously destroy the integrity of the host structure, while the third one only needs a single material and destroy the plate as small as possible. Therefore, tuning local resonance is a good approach to design the metasurface.

For the resonance based metasurface, there is an intrinsic coupled relation between the effective mass M_{eff} and effective stiffness K_{eff} of the local resonator. M_{eff} and K_{eff} are intrinsically responsible for the phase shift and transmission [18], respectively.

The coupled relation makes it very challenging to design the metasurface which supports high transmission and full phase control for transmitted waves. This can be found from the previous study [17], which obtained a low transmission efficiency of 25% by only considering the effect of M_{eff} for covering the 2π phase shift span. Recently, breaking the intrinsic coupled relation, Lee *et al*. [18] proposed a full transmission metasurface for in-plane longitudinal waves. Nevertheless, similar studies are lacking for other plate waves, such as flexural waves.

On the other hand, without considering the coupled relation, accumulating phase shift by the combination of multiple single units can also realize both high transmission and full phase control for the transmitted wave, as applied in the studies of the acoustic metasurface [11, 20]. Based on this idea, Li *et al*. [19] reported an adaptive metasurface capable of modulating A_0 Lamb waves through a combination of four single piezoelectric cells in a functional unit. However, the study did not carry out the corresponding experimental verification. Therefore, it is necessity to propose a new elastic metasurface with a simple structure and verify its deflecting functionality by the corresponding experiments.

In this paper, we propose an innovative and simple metasurface, which can support high transmission and full phase control, to deflect the incident flexural wave. The metasurface is composed of slots and three-dimensional (3D) functional units. The 3D functional units are combined with multiple slender pillars for phase shift accumulation. The 2D functional units are firstly designed, and then they are extended to the corresponding 3D ones. Furthermore, by integrating the 3D functional units, the

metasurface is theoretically designed according to the GSL. Finally, we numerically investigate wave propagation through the designed metasurface, and carry out the corresponding verification experiments.

2. Design of the pillared metasurface unit

The pillared metasurface is based on the local resonance of the pillar structure. We firstly consider a single pillar as the unit and use this unit to adjust the amplitude and phase shift of the transmitted waves by varying the pillar height. However, the pillar width in the unit needs to be particularly designed. To reduce the computation cost in the design, the 2D finite element model of a plate with the pillar unit is built in COMSOL MULTIPHYSICS software (solid mechanics module), as depicted in Fig. 1 (a). The whole pillar and plate are made of aluminum alloy, with elastic modulus of $E_{\text{alu}} = 70$ GPa, Poisson's ratio of $\nu_{\text{alu}} = 0.33$, and the density of $\rho_{\text{alu}} = 2700$ kg/m^3. The left and right boundaries of the plate are set as the perfect matched layer (PML) to avoid any reflection from the boundaries of the plate. An excitation frequency in the presented study is selected as 6 kHz, which is one of the typical excitation frequencies. For the aluminum plate with the thickness of $d = 1$ mm in the established model, the flexural wave wavelength λ is 40 mm [21]. The exciting force is applied normally on the surface of the plate (at Point A in Fig. 1 (a)). The amplitude and phase of the excited flexural wave in the far field (at Point B in Fig. 1 (a)) are examined by varying the pillar height h, while the pillar width w_0 is set as five values $w_0 = 2d,\ 4d,\ 6d,\ 8d,\ 10d$, respectively.

The transmittance is defined as the ratio of the wave amplitude in the transmitted

field (Point B) to that in the incident field. For a plate with pillars, the wave field in the incident region is a superposition of the incident field and the small reflection one. Therefore, the amplitude of pure incident field needs to be obtained in the plate without the pillar. The phase shift is obtained by subtracting the phase in Point B from the initial phase in excitation position (Point A). The transmittance and phase shift of transmitted waves along with the varying of w_0 and h are shown in Fig. 1 (b). It can be observed that the phase shift does not significantly change along with the varying of the pillar height and width. However, the transmittance increases along with the reduction of pillar width. Therefore, to obtain the high transmission, the pillar width is selected as $2d$ in the metasurface unit.

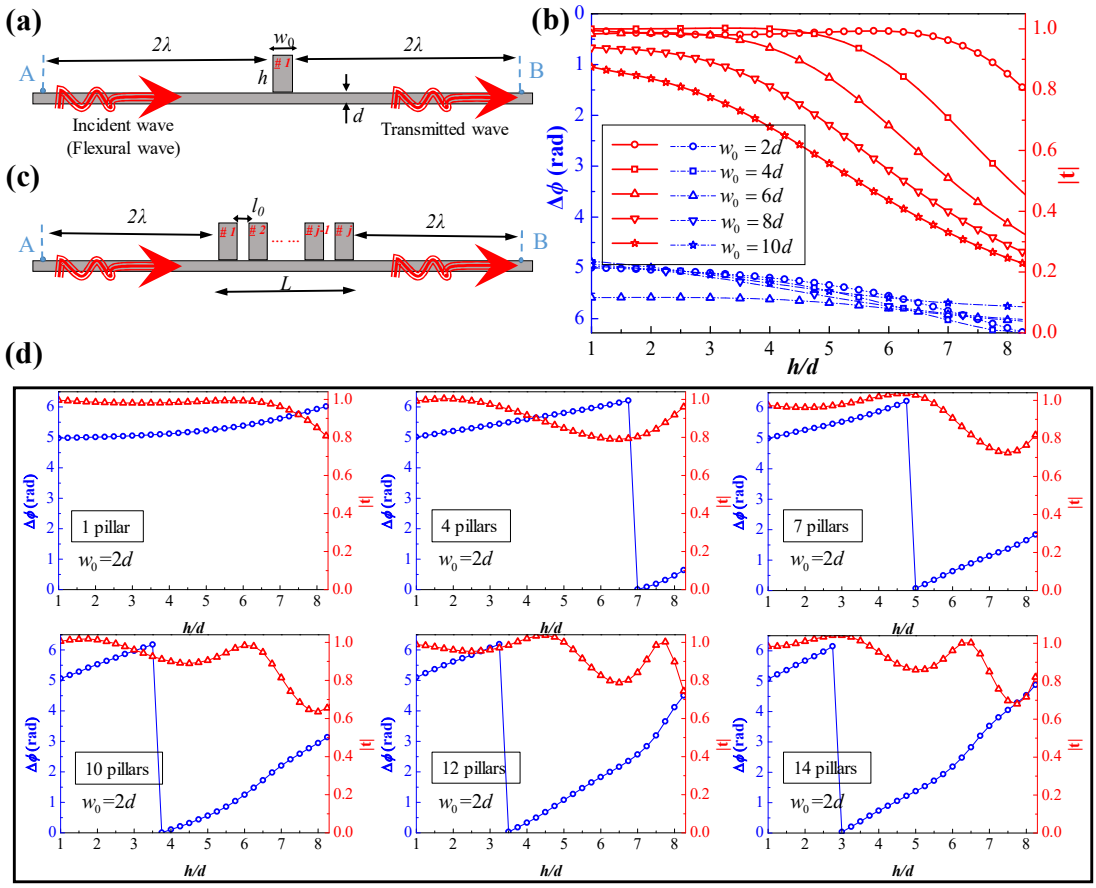

Figure 1. (a) The 2D model diagram of the plate with a single pillar; (b) Phase shift (blue dotted)

$\Delta\phi$ and transmittance (red solid) $|t|$ along with the varying of the dimensionless height h/d, while the width w_0 is set as five values $w_0 = 2d,\ 4d,\ 6d,\ 8d,\ 10d$, respectively; (c) The 2D model diagram of the plate with multiple single pillars; (d) Phase shift (blue circle) $\Delta\phi$ and transmittance (red triangle) $|t|$ along with the varying of the dimensionless height h/d, while the number of identical pillars is set as 1, 4, 7, 10, 12 and 14, for $w_0 = 2d$, respectively.

The unit must have the capability of shaping the full phase range of 2π according to the GSL. However, for the above unit with the selected pillar width of 2*d*, the phase shift span (see Fig. 1 (b)) is limited within a small range (around 0.98 rad with a high transmittance) along with the varying of the pillar height. For obtaining a full 2π phase shift span, multiple identical pillars are combined to accumulate the phase shift. The multiple identical pillars make up a functional unit, as shown in Fig. 1 (c). The number of identical pillars and the gap width between adjacent ones are denoted as *j* and l_0, respectively. The gap width l_0 is set as *d*. Subsequently, the pillar number in the unit need to be determined to extend the phase shift span. The transmittance and phase shift of transmitted waves are examined by varying the pillar height *h*, while the pillar number is set as six values *j* = 1, 4, 7, 10, 12, 14, respectively, as shown in Fig. 1 (d). It can be observed that the phase shift of transmitted waves with high transmission by varying the pillar height can span over a full 2π phase range when the pillar number is more than 12. Therefore, the pillar number is selected as 12 to constitute the sub-wavelength functional unit. In this case, its thickness (L=$35 \cdot d = 35$ mm) is less than the incident wavelength ($\lambda = 40$ mm). At this stage, we can tune the only parameter, i.e. pillar height, to realize full phase control of high transmission wave.

The above designed functional unit is embodied in its 2D model. To deflect a flexural wave, the functional unit should be designed as the corresponding 3D one in Fig. 2 (a), which can be formed by simply stretching the 2D model in Fig. 1 (c). The stretched width is denoted as w_1. The 3D functional unit can be analyzed by applying the periodic boundary conditions on the two long boundaries in the 3D strip-like model in Fig. 2 (a). The reason is that the metasurface is formed by periodically integrating different 3D functional units. Here, the formed 3D functional unit is equivalent to the corresponding 2D one after applying the periodic boundary conditions. However, slots should be cut from the 3D functional unit to separate adjacent different 3D functional units in a metasurface, as shown in Fig. 2 (b). The aim is to avoid the coupling [22] between the adjacent different 3D functional units in the integrated metasurface. The filling ratio of the slots in one functional unit is denoted as η, which is defined as dividing the slot width by the stretched width in a functional unit.

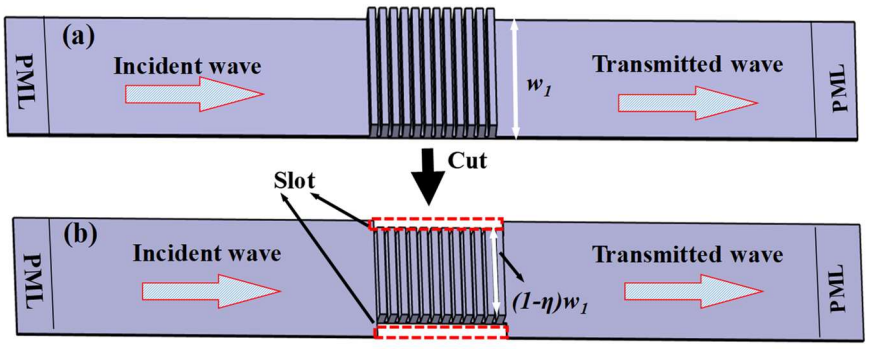

Figure 2. (a) The model diagram of the 3D functional unit without slots; (b) The model diagram of the 3D functional unit with slots.

After filling slots, the 3D functional unit structure, which can be equivalent to the corresponding 2D one, has been changed. The influence of w_1 and η on the functionality of the 3D functional unit needs to be investigated. Firstly, the pillar height

of the 3D functional unit is arbitrarily selected as $5d$. The phase shift and transmittance of the transmitted waves are obtained by varying w_1 and η, as shown in Fig. 3 (a) and (b). For comparison, the phase shift and transmittance of the transmitted wave for the corresponding 2D model without w_1 and η are marked by small circles on the right color legend in Fig. 3 (a) and (b). It can be observed that the adjusting wave effect of the 3D functional unit and that of the corresponding 2D one are same when w_1 is less than 0.8λ. The reason is that the greater the value of w_1 is, the bigger the slot is, when the filling ratio is fixed (i.e. a small value). The big slot will leads to a strong flexural wave scattering. The wave scattering affects the transmission and phase shift. Other 3D functional units with different pillar heights also satisfy the same conclusion.

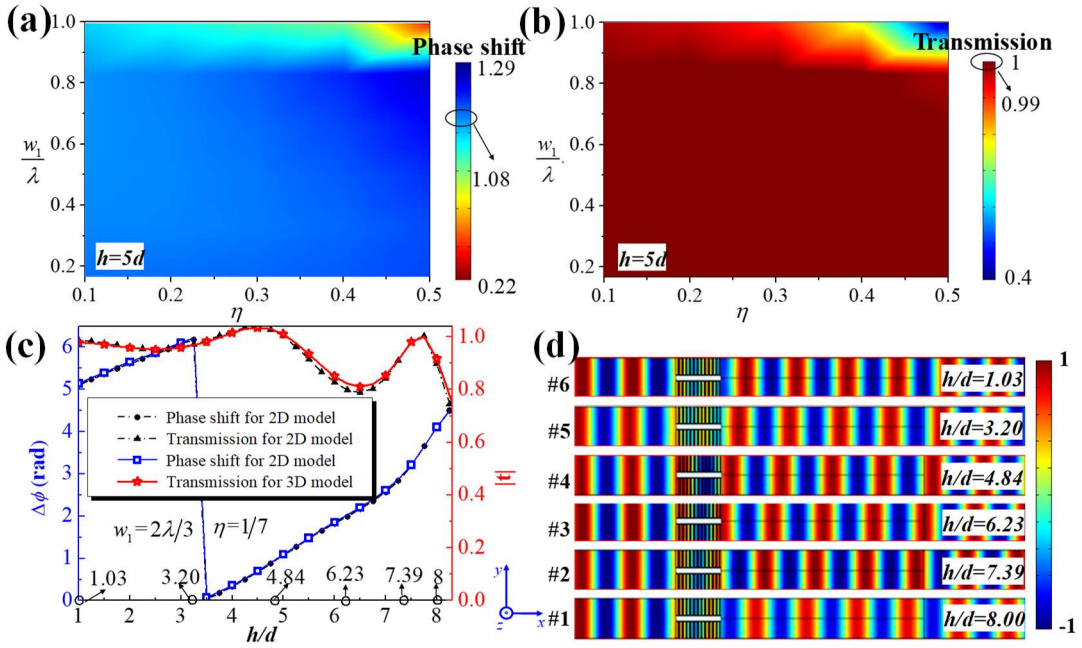

Figure 3. (a) Phase shift and (b) transmittance for the 3D functional unit along with varying the stretched width and the filling ratio of slot when the pillar height is $5d$. Phase shift and transmittance for the corresponding 2D functional unit are marked by small circles on the right color legend; (c) Phase shift $\Delta\phi$ and transmittance $|t|$ along with varying the dimensionless height h/d for the

3D functional unit. For comparison, phase shift and transmittance for the corresponding 2D functional unit are also added; (d) The corresponding out-of-plane (z component) displacement distribution for the six specific 3D functional units with the height values marked by small circles in the x axis of (c).

Based on the results shown in Fig. 3 (a) and (b), the stretched width and the filling ratio of the slots are selected as $2\lambda/3$ and 1/7, respectively, for realizing equivalence between the 3D functional unit and the corresponding 2D one. For further verifying the conclusion, the adjusting wave effect of the designed 3D functional unit is compared with that of the corresponding 2D one, as shown in Fig. 3 (c). It can be clearly observed that the phase shift and transmittance curves for the 3D functional unit have a good agreement with that of the 2D one. It demonstrates that the design of 2D functional unit is successfully extended to that of the corresponding 3D one. In Fig. 3 (c), six specific 3D functional units are selected to achieve six steps of an equally spaced phase shift to cover a full 2π range. The corresponding dimensionless heights h/d are shown by six small circles in the x axis of Fig. 3 (c). The corresponding out-of-plane (z component) displacement distributions are plotted in Fig. 3 (d). Similarly, other number of specific 3D functional units in one supercell can also be selected to cover a full 2π range.

3. Metasurface design for deflecting flexural wave

The selected 3D functional units, which cover a full 2π range, make up the individual supercell. The width of the formed supercell can be obtained as

$$W = i \cdot w_1 \tag{1}$$

where i is the number of functional units in one supercell. The metasurface is formed

by periodically integrating the supercells, as shown in Fig. 4. In one supercell, phase shift of functional units is set as increasing (decreasing is similar) along the opposite direction of the *y*-axis. Here, recalling that phase shift of one supercell covers a full 2π range, due to the wave periodicity, phase shift of the transmitted wave through the functional units linearly increases along with the opposite direction of the *y*-axis. Therefore, the spatial phase shift gradient can be described as

$$\frac{d\phi}{dy} = \frac{2\pi}{W} = \frac{2\pi}{i \cdot w_1} \tag{2}$$

According to the GSL, the theoretical refraction angle θ_t of the incident wave can be calculated by

$$\theta_t = \arcsin\left[\sin\theta_i + \frac{\lambda}{2\pi} \cdot \frac{d\phi}{dy} \right] \tag{3}$$

where θ_i is the incident angle. According to the above equation, we can adjust the phase shift gradient $d\phi/dy$ to design the arbitrarily required refraction angle of the incident wave when the incident angle is given.

Firstly, a vertical incident flexural wave is considered, i.e. $\theta_i = 0$. When the metasurface is composed of the above six selected 3D functional units, the theoretical refraction angle of the transmitted wave can be calculated to be 14.5° according to Eqs. (2) and (3). To numerically verify tunability of the metasurface, we calculate the refraction angle of the incident wave as 10.8° for the metasurface composed of the eight different functional units. It should be pointed out that the change of the unit number in one supercell will affect spatial resolution along the metasurface direction. The more the unit number in one supercell is, the higher the spatial resolution is, and vice versa.

A high spatial resolution will lead to a good quality of deflecting phenomenon [23]. The deflecting phenomenon with a good quality is that the transmitted wave can be deflected without any unwanted distortion and other diffraction waves. When the unit number in one supercell is more than six, high quality deflecting can be obtained for our design.

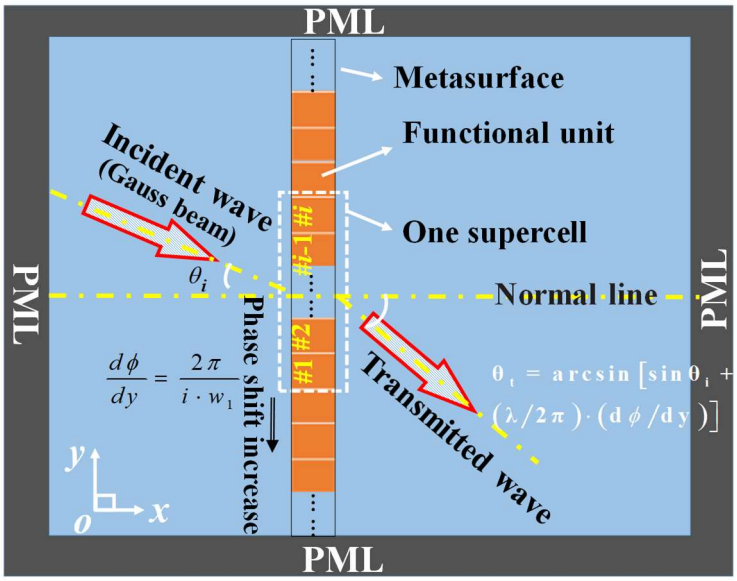

Figure 4. The schematic diagram of deflecting an incident wave by the metasurface composed of periodical supercells. One supercell has *i* functional units.

Secondly, the incident wave with an incident angle of $\theta_i = 14^{\circ}$, which is one of the typical incident angles, is considered to explore the deflecting functionality of the metasurface for oblique incident waves. For the convenience of the following experimental verification, the metasurface composed of six different functional units is considered here. According to Eqs. (2) and (3), the corresponding theoretical refraction angle of the transmitted wave can be calculated to be 29.5°. Particularly, when a negative incident angle meets with the relation $|\sin\theta_i| < (\lambda/2\pi)\cdot(d\phi/dy)$, a positive refraction angle can be obtained according to Eq. (3). It demonstrates that negative

refraction will occur. When an incident (transmitted) wave and the one in Fig. 4 are on the different sides of the normal line, the incident (refraction) angle can be defined as a negative incident (refraction) angle. The negative refraction means that the incident and transmitted angle are on the same side of the normal line. As a typical example to realize negative refraction, the incident angle is set as $\theta_i = -5^\circ$, the corresponding theoretical refraction angle is calculated to be 9.4°.

4. Flexural wave deflection - numerical simulations

The numerical simulations are implemented to demonstrate the deflecting functionality of designed metasurface for flexural waves. The simulation model is built according to the model in Fig. 4, and the width of designed metasurfaces is fixed as $24\,w_1$. Firstly, the black line, which is perpendicular to the prescribed incident wave direction, is built at the left side of the simulation domain, as shown in Fig. 5. Then, prescribed displacements in the *z*-direction are applied along the black line to generate flexural wave Gaussian beam. The distribution function of prescribed displacement is $w_y = \exp\left\{-[(\mathrm{y}-\mu)/\cos\theta_i]^2/(2\delta^2)\right\}$, where μ is the ordinate of the midpoint in the black line and the variance δ determines the width of Gaussian beam.

The flexural wave fields are obtained in terms of out-of-plane displacements (*z* component) at the slice located in the upper surface of the plate. The numerical results are shown in Fig. 5 and the corresponding phase shift gradients of the metasurfaces are inserted in the bottom of the figures. It can be clearly observed that the vertical and oblique incident waves have been deflected by the designed metasurface and the negative refraction appears in the transmitted field. For comparison, the theoretical

predictions (see arrows in Fig. 5) are superimposed on the full wave fields obtained from the numerical simulations. It can be observed that the theoretical refraction angles have an excellent agreement with the numerical ones. It confirms that the designed metasurface has the effectively deflecting functionality for vertical and oblique incident flexural waves.

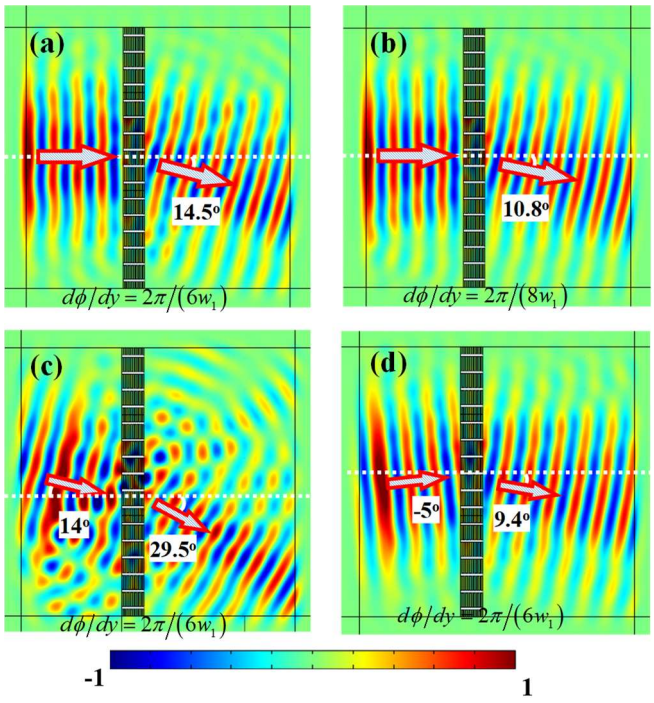

Figure 5. Wave fields for vertical incident flexural wave Gaussian beams through two metasurfaces with different phase shift gradients: (a) $d\phi/dy = 2\pi/(6w_1)$, (b) $d\phi/dy = 2\pi/(8w_1)$. Wave fields for oblique incident flexural wave Gaussian beams with different incident angles: (c) $\theta_i = 14^\circ$, (d) $\theta_i = -5^\circ$ through the metasurface with phase shift gradient $d\phi/dy = 2\pi/(6w_1)$.

5. Flexural wave deflection - experiment

In order to further validate the deflecting functionality, we select above designed metasurface composed of six different functional units to perform a set of experimental investigations. To accurately fabricate the metasurface, the Computer Numerical

Control (CNC) milling machine with a manufacturing precision of 0.01 mm is adopted. Both the metasurface structure and 1-mm-thick aluminum plate are directly obtained by milling a thick aluminum plate (800 mm × 800 mm × 10 mm), as shown in Fig. 6. The enlarged view of one supercell in the metasurface sample is shown in the top of Fig. 6. An array of four piezoelectric patches (19.5 mm × 22 mm × 0.3 mm) is bonded on the surface of the plate as actuators. The spacing of adjacent piezoelectric patches is half of the piezoelectric patch width. By rotating the direction of the bonded piezoelectric patch array, we can get the different incident angles, such as obtaining the incident angle 14° and -5°, as shown in Fig. 6.

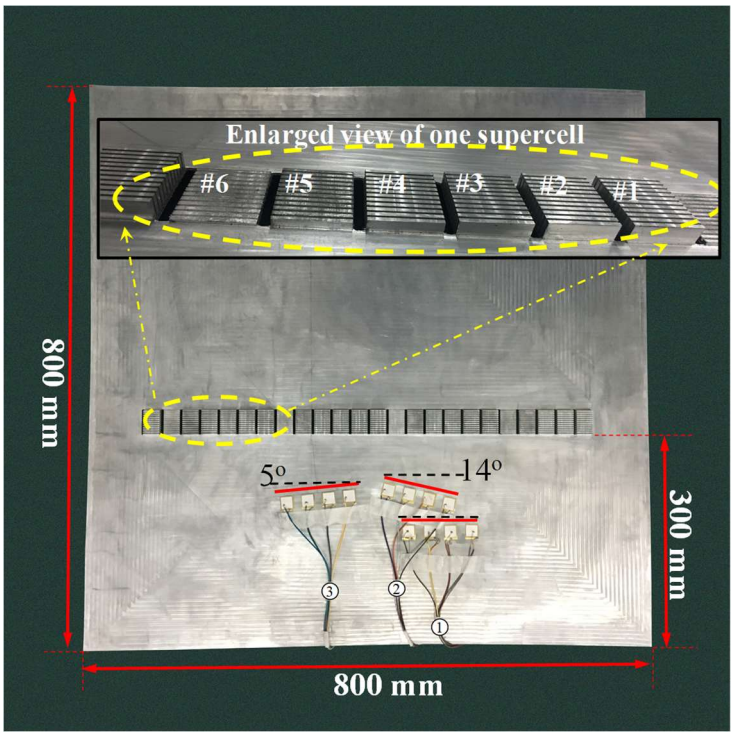

Figure 6. The model diagram of the test piece.

The test set-up and signal flow chart are shown in Fig. 7 (a) and (b), respectively. The thin test piece is fixed by the lines in four corners of test piece and the bracket in the bottom of test piece. A layer of blue-tack is glued on the boundary edges in order to

minimize reflections from the outer boundary of the test piece. With the controlling of the waveform editor (based on Labview Software), the signal generator (Agilent 33220A) generates a 5-cycle tone burst $w_t = A_0\left[1-\cos\left(2\pi f_c t/5\right)\right]\sin\left(2\pi f_c t\right)$, where $f_c = 6$ kHz is the central frequency. The piezoelectric patches are driven by a power amplifier (HVPA05). The amplified voltage for the two middle piezoelectric patches is two times of that for the two external piezoelectric patches. The bonded piezoelectric patch array can approximately excite the flexural wave Gaussian beam. The wave fields are measured by a PSV-400 scanning laser Doppler vibrometer, which is perpendicularly aimed to the plate surface in order to scan the out-of-plane displacement fields. In measurement mode of the frequency domain, the full field measurements are obtained by scanning about 7 points per flexural wavelength in the incident and transmitted areas, except for the metasurface region.

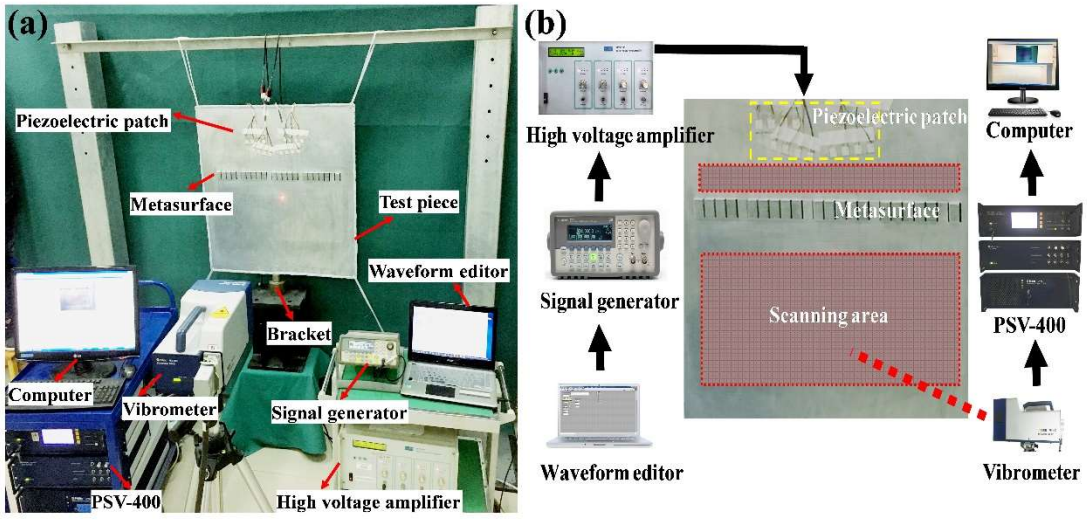

Figure 7. (a) Test set-up; (b) Signal flow chart.

The full field experimental measurements for the flexural waves in a plate with the metasurface are shown in Fig. 8 (b)-(d). For comparison, the test result for the flexural waves in a plate without the metasurface is also given in Fig. 8 (a). From the

four test results, it is found that the designed metasurface can abnormally deflect both the vertical and oblique incident flexural waves. The experimentally observed angles are 13.8°, 25.6° and 10.3° in Fig. 8 (b)-(d), respectively, recalling that the corresponding theoretical angles are 14.5°, 29.5° and 9.4°. More importantly, all the experimental test results are in good agreement with both the theoretical and numerical results. The small error mainly comes from the angle of the incident wave excited by the bonded piezoelectric patch array.

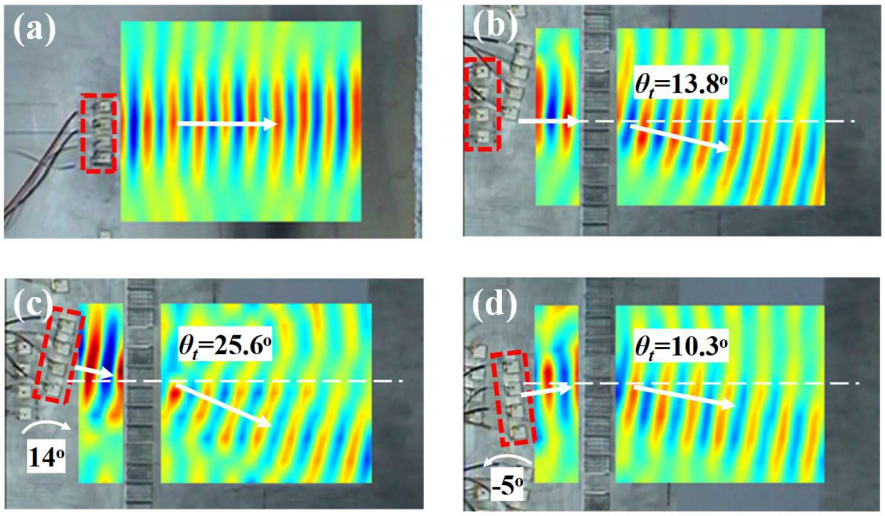

Figure 8. Test results. (a) Referenced transmitted wave field in a plate without the metasurface; Incident and transmitted wave fields in a plate with the metasurface for the incident angles: (b) 0°, (c) 14° and (d) -5°.

6. Conclusions

We propose and design a simple pillared metasurface to abnormally deflect vertical and oblique incident flexural waves based on phase accumulation. The designed metasurface supports high transmission and full phase control for flexural waves. It is shown that the design of 3D functional units can be guided from that of the corresponding 2D ones for simplicity. We have numerically and experimentally verified

the functionality of deflecting vertical and oblique incident flexural waves in the theoretically designed metasurface. The results show that the proposed metasurface is effective for deflecting the vertical and oblique incident flexural waves in the sub-wavelength regime. In particular, negative refraction is also realized. The designed metasurface with a simple structure can lead to promising practical application based on flexural wave steering in many fields, such as ultrasonic detection, energy harvesting, and vibration control.

Acknowledgements

This project is supported by the National Natural Science Foundation of China (Grant No. 11602194) and Aeronautical Science Foundation of China (Grant No. 20161553016).

References

[1] Liu Z Y, Zhang X X, Mao Y W, Zhu Y Y, Yang Z Y, Chan C T and Sheng P 2000 Locally resonant sonic materials Science 289 1734-1736

[2] Li J F, Zhou X M, Huang G L and Hu G K 2016 Acoustic metamaterials capable of both sound insulation and energy harvesting Smart Mater. Struct. 25 045013

[3] Zhou W L, Wu Y and Zuo L 2015 Vibration and wave propagation attenuation for metamaterials by periodic piezoelectric arrays with high-order resonant circuit shunts Smart Mater. Struct. 24 065021

[4] Cummer S A, Christensen J and Alu A 2016 Controlling sound with acoustic metamaterials Nat. Rev. Mater. 1 16001

[5] Yu N F, Genevet P, Kats M A, Aieta F, Tetienne J P, Capasso F and Gaburro Z 2011 Light Propagation with Phase Discontinuities: Generalized Laws of Reflection and Refraction Science 334 333-337

[6] Kildishev A V, Boltasseva A and Shalaev V M 2013 Planar Photonics with Metasurfaces Science 339

[7] Yu N F and Capasso F 2014 Flat optics with designer metasurfaces Nat. Mater. 13 139-150

[8] Zhao J J, Li B W, Chen Z N and Qiu C W 2013 Redirection of sound waves using acoustic metasurface Appl. Phys. Lett. 103 151604

[9] Zhu X, Li K, Zhang P, Zhu J, Zhang J, Tian C and Liu S C 2016 Implementation of dispersion-free slow acoustic wave propagation and phase engineering with helical-structured metamaterials Nat. Commun. 7 11731

[10] Qi S B and Assouar M B 2017 Acoustic energy harvesting based on multilateral metasurfaces Appl. Phys. Lett. 111 243506
[11] Li Y, Qi S B and Assouar M B 2016 Theory of metascreen-based acoustic passive phase darray New J. Phys. 18 1367-2630
[12] Xu Y L, Li Y, Cao L Y, Yang Z C and Zhou X L 2017 Steering of SH wave propagation in electrorheological elastomer with a structured meta-slab by tunable phase discontinuities AIP Adv. 7 095114
[13] Su X, Lu Z and Norris A N 2018 Elastic metasurfaces for splitting SV- and P-waves in elastic solids J. Appl. Phys. 123 091701
[14] Shen X, Sun C-T, Barnhart M V and Huang G 2018 Elastic wave manipulation by using a phase-controlling meta-layer J. Appl. Phys. 123 091708
[15] Cao L Y, Yang Z C and Xu Y L 2018 Steering elastic SH waves in an anomalous way by metasurface J. Sound. Vib. 418 1-14
[16] Liu Y Q, Liang Z X, Liu F, Diba O, Lamb A and Li J S 2017 Source Illusion Devices for Flexural Lamb Waves Using Elastic Metasurfaces Phys. Rev. Lett. 119 034301
[17] Zhu H and Semperlotti F 2016 Anomalous Refraction of Acoustic Guided Waves in Solids with Geometrically Tapered Metasurfaces Phys. Rev. Lett. 117 034302
[18] Lee H, Lee J K, Seung H M and Kim Y Y 2017 Mass-Stiffness substructuring of an elastic metasurface for full transmission beam steering J. Mech. Phys. Solids 112 577-593
[19] Li S, Xu J and Tang J 2018 Tunable modulation of refracted lamb wave front facilitated by adaptive elastic metasurfaces Appl. Phys. Lett. 112 021903
[20] Xie Y B, Wang W Q, Chen H Y, Konneker A, Popa B I and Cummer S A 2014 Wavefront modulation and subwavelength diffractive acoustics with an acoustic metasurface Nat. Commun. 5 5553
[21] Achenbach J D 1973 Wave Propagation in Elastic Solids (Amsterdam: North-Holland Press) pp 254–256
[22] Jin Y B, El Boudouti E, Pennec Y and Djafari-Rouhani B 2017 Tunable Fano resonances of Lamb modes in a pillared metasurface J. Phys. D. Appl. Phys. 50 425304
[23] Li Y, Jiang X, Liang B, Cheng J C and Zhang L K 2015 Metascreen-based acoustic passive phased array Phys. Rev. Appl. 4 2331-7019